Seventh International Conference on CFD in the Minerals and Process Industries
CSIRO, Melbourne, Australia
9-11 December 2009

THE EFFECT OF GAS DYNAMICS ON HOPPER DISCHARGE RATES

James E. HILTON[1*], Lachlan R. MASON and Paul W. CLEARY

[1] CSIRO Mathematical and Information Sciences, Clayton, Victoria 3169, AUSTRALIA
*Corresponding author, E-mail address: James.Hilton@csiro.au

ABSTRACT

Hopper discharge is one of the oldest and most widely studied problems in granular flow owing to the simple set-up and geometry of the system. It has been extensively investigated both experimentally and computationally, and many granular flow theories use hopper discharge as a benchmark for validation. Most simulations neglect the effect of the interstitial gas, as the gas phase is assumed to have little influence on the dynamics of the particles. However, at small length scales drag forces significantly alter flow rates. We investigate these gas flow effects at different hopper size scalings using a coupled Discrete Element Method and pressure-gradient-force Navier Stokes solution method. We show excellent agreement between our results and various hopper flow theories, and demonstrate the strong influence of the gas flow on the discharge rate of the hopper at small length scales. We show that granular dilation occurs which is consistent with the granular free-fall arch theory at the hopper outlet, accompanied by a sharp gas pressure gradient opposing the particle motion. We also find a pre-dilation region prior to the granular arch corresponding to a granular dilatancy point. Our findings enable both an improved understanding of the fluid-gas flow interaction and the evaluation of strategies for specific industrial installations.

NOMENCLATURE

A	Particle cross sectional area
A_W	Mass flow area
C_D	particle drag coefficient
C	flow rate coefficient
C_0	Beverloo flow rate coefficient
d	particle diameter
D	hopper diameter
D_0	hopper outlet orifice diameter
f_g	gas volume flow rate = $\|\mathbf{u}\|A_W$
f_s	particle volume flow rate = $\|\mathbf{v}\|A_W$
$\mathbf{f}$	particle to gas coupling body force
g	gravitational acceleration
H	hopper fill height
k	Beverloo annulus constant
K	Carman-Kozeny constant
p	pressure
$\mathbf{F}$	particle force
$\mathbf{T}$	particle torque
$\mathbf{u}$	gas velocity
$\mathbf{u_r}$	particle slip velocity
$\mathbf{v}$	particle velocity
V	particle volume
W	mass flow rate
$\delta\mathbf{x}$	particle overlap
α	gas to solid flow speed ratio
ε	voidage fraction
χ	hopper stagnant region angle from horizontal
μ	particle friction
ρ_f	gas density
ρ_p	particle density
ρ_b	bulk particle density = $(1-\varepsilon)\rho_p$
η	viscosity
$\boldsymbol{\omega}$	particle spin vector

INTRODUCTION

Effective handling of granular materials is of significant importance to many industrial processes. Large-scale hoppers are used for storage and transportation of coarse feed stocks in chemical and food manufacture while the flow characteristics of fine powders affect process design in the pharmaceuticals industry. The flow rate of solids from a hopper has been known to be independent of the fill height, H, since Janssen's results derived in 1895. The flow rate is also known to be independent of the hopper diameter, D, given the respective restrictions $H > 2.5D$ and $D > 2.5D_0$, where D_0 is the outlet diameter (Ketchum 1929; Brown and Richards, 1960). Beverloo et al. (1961) used the restriction of constant Froude number along with experimental data to give an expression for flow rate as a function of particle and orifice diameter, although a relation of this type had been suggested as early as 1852 (Seville, 1997, p332). This expression was later modified to take into account gas effects by Crewdson *et al*. (1977) by incorporating a pressure gradient as a body force.

The hopper mass flow rate is determined by granular dynamics within the vicinity of the orifice (Nedderman *et al*., 1982). Brown (1960, 1961) used this local effect to introduce the concept of the 'free fall arch'. This is assumed to be a spherical section spanning the hopper outlet where the granular flow transforms from dense phase flow, with long lasting frictional collisions, to dilute phase flow, with intermittent instantaneous collisions. In the dilute region friction can be neglected and forces due to interstitial pressure gradients become important. Using this concept Brown postulated that the total mechanical energy per unit mass decreases along a flow streamline until it is minimised at the free-fall arch. Although inconsistencies with Brown's theory have been stated (Wieghardt, 1975; Kaza and Jackson 1984) the theory has been successfully applied and extended by Altenkirch *et al*. (1981) to incorporate the interaction between solids and interstitial fluid. Barletta *et al*. (2004), later expanded the theory further to include the effects of solids dilation.

A review of other semi-theoretical approaches for the inclusion of interstitial fluid drag effects is presented by Nedderman *et al*. (1983). A further group of correlations include a macroscopic pressure difference term typically measured between the orifice and a tapping on the hopper wall (Resnick, 1972; Bulsara *et al*., 1964; McDougall and Evans, 1966; Leung *et al*., 1978). Seville *et al*., (1997) state that this approach cannot be used to derive an

expression for flat-bottomed hoppers, such as the ones used in this study, as evaluation of the pressure gradient requires a closed form solution of Laplace's equation. Nedderman *et al*. outline a possible solution method under the assumptions of constant voidage in the laminar regime.

Hopper flow has been extensively computationally investigated using the Discrete Element Method (DEM). Recent papers include Zhu and Yu (2004), who investigated the dependency of solids mass flow rate on orifice diameter using a flat-bottomed cylindrical geometry scaled by a fixed particle diameter. Simulation results correlated well with the Beverloo equation. Anand *et al*. (2008) utilised DEM to investigate the dependence of mass flow rate on particle properties in a pseudo three-dimensional angled hopper. Wu *et al*. (2009) extended this approach to investigate the effects of polydisperse particle size distributions. In comparison to mono-disperse systems, poly-dispersity resulted in a decrease in mass flow rate for small orifice diameters due to the presence of larger particles aiding an obstructive 'bridging action'. The majority of DEM simulations assume spherical particle geometry, however Cleary and Sawley (2002) have shown that particle shape can significantly alter hopper mass flow rates. Using a superquadric formulation, it was found that particles of large aspect ratio give a flow rate reduction of up to 30% over spherical particles. Sphero-disks (Lia *et al*., 2004) and spherical clusters (Abou-Chakra, *et al*., 2004) have also been considered.

The effect of gas flow on hopper discharge has, however, been largely neglected. Eulerian-Lagrangian coupling of gas and solid phases was introduced to DEM by Tsuji *et al*. (1993) in the context of two-dimensional fluidised beds. Langston *et al*. (1995) investigated the effects of drag on particle flow rate in a shallow angled hopper for closed-top air-retarded gravity flow and open-top air-assisted discharge. For the air-retarded case solids flow rates were observed to decrease with decreasing effective particle density. For the air-assisted case an increase in the forcing over-pressure led to a steady increase in particle velocity magnitudes and increasing wall stresses. A solid discharge ratio from air-assisted simulation data was compared to a continuum result of Nedderman (1992), although no comparison to theoretical correlations concerning the effect of particle size scale on gas-drag effects was presented. The assumption of radial gas flow was used, and interstitial fluid effects were modelled by varying the effective particle density.

More recently, Snider (2007) simulated sub 500μm particle flow in a cylindrical flat-bottomed hopper using the computational particle fluid dynamic method. Simulated mass flow rates agreed with corresponding experimental results for fine sands, although only one size scaling was investigated. Guo *et al*. (2009) used DEM to investigate the effects of interstitial gas drag on fine particles in die filling. A pseudo two-dimensional flat-bottomed geometry was used and both particle diameter and density were systematically varied. For vacuum conditions, simulation results for mono-disperse particles were observed to have an average dimensionless flow rate agreeing well with an expression derived from dimensional analysis by Beverloo (1961). When gas modelling was included small particle diameters and low densities both gave a lower mass flow rate.

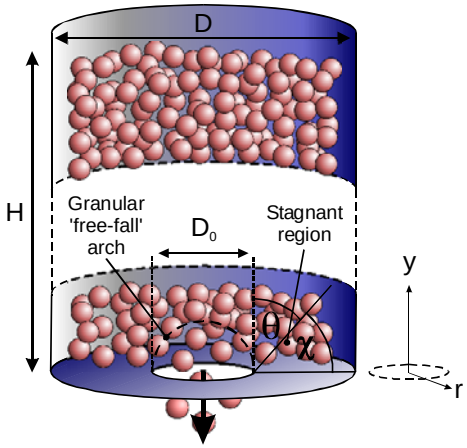

Figure 1: Parameters for flat-bottomed hopper geometry.

In our simulations we systematically vary the length scaling of the hopper to ascertain the point at which gas effects become important. We use the same particle set-up at a range of different scalings with and without gas flow, so that any differences between the simulations are due only to the imposed scaling.

THEORETICAL HOPPER FLOW RATES

In the following section we provide a brief overview of theoretical hopper mass flow predictions which we will use to compare to our simulation results. The simpler case of granular flow without gas effects is presented first, followed by the outline of a derivation for mass flow based on Altenkirch *et al*. (1981), incorporating the effects of interstitial gas.

Flow Rates Without Gas Effects

The dynamics of a particle falling in a fluid is governed by the ratio of drag force on the particle, $\approx \frac{1}{2} A \rho_f u_r^2 C_D$, to the gravitational force, $\approx V \rho_p g$. This ratio is proportional to the product of the ratio of fluid to solid density and the square root of the Froude number. For a spherical particle this gives:

$$k = \frac{3}{8} C_D \frac{\rho_f}{\rho_p} \frac{u_r^2}{Lg} = \frac{3}{8} C_D \frac{\rho_f}{\rho_p} \sqrt{Fr} \qquad (1)$$

For a fixed density ratio the system is therefore governed by the Froude number, *Fr*. If *Fr* is assumed constant and the velocity is taken from the mass flow rate, $W = \rho_b |u_r| A_W$, then the following relation holds:

$$W = C \rho_b \sqrt{g} D_0^{5/2} \qquad (2)$$

where D_0 is the characteristic length scale in the system. Beverloo *et al.* (1961) investigated this relation using a wide range of experimental data for flat bottomed hoppers. Although the slope was found to be correct, there was a non-zero intercept on the order of $k \times d$, where $k \approx 1.5$. This was explained by an 'empty annulus on the order of *k* particle diameters, through which no solids flow can occur'. Eq. (2) was therefore modified to:

$$W = C r_b \sqrt{g} \left(D_0 - k d \right)^{5/2} \qquad (3)$$

where the parameter $C = C_0 \approx 0.58$.

Flow Rates Incorporating Gas Effects

Eq. (3) agrees well with experimental flow rates for particle diameters greater than 500 μm. However, for smaller sized particles interstitial pressure gradients

become important and the flow impeding effects of gas drag cannot be neglected. This leads to a significant deviation between the correlation and experimental results. Flow rates are observed to decrease with decreasing diameter, but the effect of decreasing d in Eq. (3) is to increase the predicted mass flow rate of solids.

Brown (1961) approached the hopper flow problem by expressing the system in an equivalent thermodynamic context and applying a minimum energy argument. The system is divided into a frictional flow part and a dilute flow part, divided by a free fall arch spanning the orifice. The mechanical energy per unit mass is given by:

$$e = \frac{p}{\rho} + \tfrac{1}{2}v^2 + gr\cos\theta \tag{4}$$

This energy is assumed to be a minima on this arch. This argument was extended by Altenkirch *et al*. (1981) to both a solid and a gas phase, giving a total energy of the form:

$$e = \frac{p}{\rho_b} + \tfrac{1}{2}v_s^{\,2} + gr\cos\theta \tag{5}$$

Assuming the energy is a minimum at the free-fall arch and this arch is at $r = D_0/2$, along with the assumption of radial solids velocity:

$$v_s(r,\theta) = \frac{f_s(\theta)}{r^2} \tag{6}$$

gives:

$$\frac{1}{\rho_b}\frac{dp}{dr}\bigg|_{r=R_0} + 64\frac{f_s(\theta)^2}{D_0^5} + g\cos\theta = 0 \tag{7}$$

where f_s is some radial volume flow function to be determined. The assumption of the free-fall arch at $D_0/2$ is the upper limit of the minimum energy surface (Brown, 1961) and has been experimentally demonstrated to be a valid assumption for simplified flow theories, in which a sharp transition between the two flow regimes is assumed (Harmens, 1963; Donsi *et al*.,1997). The mass flow rate of solids can then be determined by integration of the radial flow field over a spherical surface of half-angle β:

$$W = 2\pi\rho_b\int_0^{\beta} f_s(\theta)\sin\theta d\theta \tag{8}$$

Altenkirch also makes the assumption of radial gas flow and that the gas and solid volume flow rates are linearly related by:

$$f_g(\theta) = \alpha\frac{1-\varepsilon}{\varepsilon}f_s(\theta) \tag{9}$$

where f_g is the gas radial flow function and α is the ratio of gas to solid flow rates. This allows the pressure gradient to be expressed from the Carman-Kozeny equation:

$$\frac{\partial p}{\partial r} = \frac{K\eta}{d^2}\left(\frac{1-\varepsilon}{\varepsilon}\right)^2 |u_r| \tag{10}$$

as:

$$\frac{dp}{dr} = \frac{K\eta}{d^2}\left(\frac{1-\varepsilon}{\varepsilon}\right)^2\left\{1-\frac{\alpha(1-\varepsilon)}{\varepsilon}\right\}\frac{f_s(\theta)}{r^2} \tag{11}$$

Substitution of this expression for the pressure gradient into Eq. (7) and applying the integration given in Eq. (8) gives the flow rate constant in Eq. (3) as:

$$C = \frac{\pi}{6}\left[\frac{\left(\gamma^2+1\right)^{3/2} - \left(\gamma^2+\cos\beta\right)^{3/2} + \frac{3}{2}\gamma\left(\cos\beta - 1\right)}{\sin^{5/2}\beta}\right] \tag{12}$$

where:

$$\gamma = \frac{K\eta\sqrt{D_0}}{4\rho_b d^2\sqrt{g}}\left(\frac{1-\varepsilon}{\varepsilon}\right)^2\left\{1-\frac{\alpha(1-\varepsilon)}{\varepsilon}\right\} \tag{13}$$

For flat-bottomed hoppers, such as the ones used in this study, β is set to equal to χ = 45°, where χ is commonly assumed to be 45° in the absence of further information (Anand *et al*., 2008), resulting in:

$$C = \frac{\pi}{6}\left(\frac{2}{\sqrt{2}}\right)^{5/2}\left[\left(\gamma^2+1\right)^{3/2} - \left(\gamma^2+\frac{\sqrt{2}}{2}\right)^{3/2} + \tfrac{3}{4}\gamma\left(\sqrt{2}-2\right)\right] \tag{14}$$

The mass flow rate is therefore a function of empirical parameters K and α only. The flow ratio α can be measured, giving the only empirical constant as K, which is taken to be 180. Further assumptions can be applied to derive a value for α (Barletta *et al*., 2003), although in our simulations this value is measured from the relative flow rates.

COMPUTATIONAL MODEL

We use a Lagrangian approach for particles called the Discrete Element Method (DEM), which was formulated by Cundall and Strack (1979). DEM has been applied to simulate a wide range of industrial processes (Cleary, 2004, 2009). This is coupled to a Eulerian fluid model for gas flow through a porous bed. The first coupling of this type was originally carried out by Tsuji (1993), who investigated a two-dimensional gas-solid fluidised bed of spherical particles. We use a pressure gradient force (PGF) DEM-gas formulation shown by Kafui (2002) to give the best agreement with empirical pressure drop and gas velocity data.

Drag Forces

The drag force exerted by the gas on a particle in a multi-particle system with corrections due to Di Felice (1994) is:

$$\mathbf{F}_D = \tfrac{1}{2}C_d\rho_f|\mathbf{u}_r|^2\varepsilon^{-\kappa}A_\perp\mathbf{u}_r \tag{15}$$

where χ is given by:

$$\kappa = 3.7 - 0.65\exp\left\{-\tfrac{1}{2}\left(1.5-\log\mathrm{Re}\right)^2\right\} \tag{16}$$

We use the drag coefficient given by Holzer *et al.* (2008) for single spherical particles:

$$C_d = \frac{27}{\mathrm{Re}} + 0.42 \tag{17}$$

Particles are also subject to Stokesian rotational drag, given by:

$$\mathbf{T}_D = \pi\eta d^3\boldsymbol{\omega}_r \tag{18}$$

Particle Motion Equations

The particle-particle contact force, $\mathbf{F}_{ci}$, is determined by the particle overlap using a soft-sphere linear spring, dashpot and slider approximation. The linear and angular accelerations are numerically integrated for each particle i. These are given by:

$$m_i\frac{d\mathbf{v}_i}{dt} = \mathbf{F}_{ci} + \mathbf{F}_D + \mathbf{F}_P + m_i\mathbf{g} \tag{19}$$

$$I_i\frac{d\boldsymbol{\omega}_i}{dt} = \mathbf{T}_{ci} + \mathbf{T}_D \tag{20}$$

The forces consist of a solid particle-particle contact force, $\mathbf{F}_{ci}$, as well as the fluid-particle interaction forces $\mathbf{F}_D$, the gradient of the fluid pressure, $\mathbf{F}_P$, and the gravitational force. The torque consists of the drag torque plus the particle-particle coupling torque, $\mathbf{T}_{ci}$.

Fluid Equations

The constitutive equations for the PGF gas flow model through a porous bed were derived by Anderson and Jackson (1967), and given by Kafui as:

$$\frac{\partial\left(\varepsilon\rho_f\right)}{\partial t}+\nabla\cdot\left(\varepsilon\rho_f\mathbf{u}\right)=0 \tag{21}$$

$$\frac{\partial\left(\varepsilon\rho_f\mathbf{u}\right)}{\partial t}+\nabla\cdot\left(\varepsilon\rho_f\mathbf{u}\mathbf{u}\right)=-\varepsilon\nabla p-\mathbf{f}_{fp}-\nabla\cdot\left(\varepsilon\boldsymbol{\tau}\right)+\varepsilon\rho_f\mathbf{g} \tag{22}$$

These can be re-formulated for the superficial gas velocity $\mathbf{u}' = \varepsilon\mathbf{u}$ in the system by assuming the gas density is constant. This gives:

$$\frac{\partial\varepsilon}{\partial t}=-\nabla\cdot\mathbf{u}' \tag{23}$$

And expression (22) becomes:

$$\frac{\partial\mathbf{u}'}{\partial t}+\frac{1}{\varepsilon}\left(\mathbf{u}'\cdot\nabla\right)\mathbf{u}'+\mathbf{u}'\nabla\cdot\frac{\mathbf{u}'}{\varepsilon}= -\frac{1}{\rho_f}\left[\varepsilon\nabla p-\mathbf{f}_{fp}-\nabla\cdot\left(\varepsilon\boldsymbol{\tau}\right)\right]+\varepsilon\mathbf{g} \tag{24}$$

The stress tensor is given by:

$$\boldsymbol{\tau}=-\eta\left[\left(\nabla\frac{\mathbf{u}'}{\varepsilon}+\nabla\frac{\mathbf{u}'^{T}}{\varepsilon}\right)-\frac{2}{3}\left(\nabla\cdot\frac{\mathbf{u}'}{\varepsilon}\right)\mathbf{I}\right] \tag{25}$$

where $\mathbf{I}$ is the identity tensor. These expressions are discretised onto a Cartesian grid filling the simulation domain.

The procedure for the numerical calculation is firstly to determine the porosity at the new time step by calculating the volume distribution from the DEM simulation. The velocity field is then calculated using Eq. (23), which gives the rate of change of porosity as divergence of the velocity, and Eq. (24) which gives the velocity field at the next timestep. Eq. (24) is solved using a variation of the pressure correction method.

The porosity is explicitly calculated from the DEM simulation at each timestep. To simulate the effect of the hopper, zero velocity boundary conditions are imposed on cells within the domain intersecting the hopper walls.

EFFECT OF SCALING

A range of simulations was carried out at different length scalings of the same set-up. The base set up was H = 10.0 m, D_0 = 1.0 m, D = 3.0 m and d = 0.125 m (= D_0/8), for a closed-top hopper. This was chosen to ensure that the bed filling height and the ratio of particle diameter to orifice diameter did not affect the particle outflow rate. The grid resolution was 15 × 120 × 15, giving a cell size of 200mm and a ratio of cell to particle diameter of 1.6. The mass flow was measured through the plane 1 m vertically below the orifice. The simulation was scaled by a factor s, given in table 1, which was applied to all parameters in the simulation that are dependant on length. The constants used in the simulation and theoretical models are given in table 2. The particle and gas volume flow rates just below the outlet for the scaling of s = 1.0 were measured as a gas flow rate of ~1.0 m/s and particle flow rate of ~1.5 m/s. This gives α = 2/3, which was assumed to hold for the other scalings. The average voidage fraction over the outlet was measured as 0.48, which was also assumed to hold for all scalings.

Scaling factor, s	d
1.0	125 mm
1.0×10^{-1}	12.5 mm
1.0×10^{-2}	1.25 mm
5.0×10^{-3}	625 μm
2.5×10^{-3}	312.5 μm
1.0×10^{-3}	125 μm
7.5×10^{-4}	93.75 μm
5.0×10^{-4}	62.5 μm

Table 1: Scaling factor and particle diameter.

Both the particle velocity and gas velocity were found to be parallel at steady state in the centre of outlet with a thin annular gas backflow around the outlet. This is can be seen in Fig. 2, where a plot of the particles and a plot of the gas velocity field are shown at t = 2.0 s for a scale factor s = 1.0. The colours represent speed with red being 10 m/s in the plot of the particles and red being 1 m/s in the plot of the velocity field.

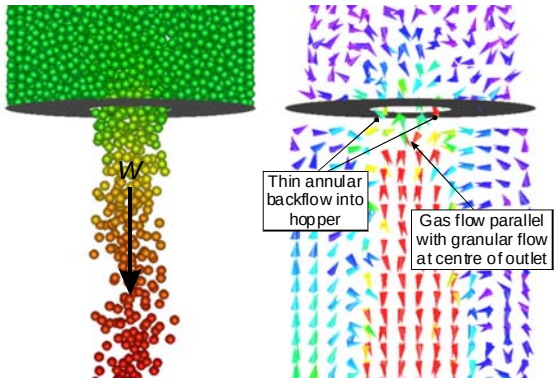

Figure 2: Particles (left) and gas velocity vectors (right) at time t = 2.0 s for a scale factor s = 1.0.

Parameter	Value
Carman-Kozeny Coefficient, K	180
Angle of Stagnant Region, χ	π/4
Beverloo Constant, C_0	0.58
Beverloo Diameter Constant, k	1.5
Gravity Magnitude, g	9.8
Gas Viscosity, η	1.8×10^{-5}
Particle Friction, μ	0.3
Particle Density, ρ_p	2700

Table 2: Configuration constants.

Fig. 3 shows the predicted flow rates at different scalings. The Beverloo relation, Eq. (3), which does not incorporate gas effects, and the Altenkirch relation, Eq. (15), which includes gas effects are also plotted. There is an excellent correlation between the theoretical and simulated flow rates. For scale factors of 0.01 and greater the air has no effect on the flow rate and the Beverloo and Altenkirch relations give very close theoretical values which match with the simulations. The upper inset of Fig. 3 shows a more detailed plot of the lowest three scaling

factors. Fig. 4 shows the percentage difference in flow rates, and it can be seen that the inclusion of gas effects in the system significantly affects the hopper discharge rate at small length scales. At the lowest scaling considered, s = 0.0005 with particle diameter 62.5 μm, there is a ~50% reduction in the particle mass flow rate with gas compared to the flow rate without gas.

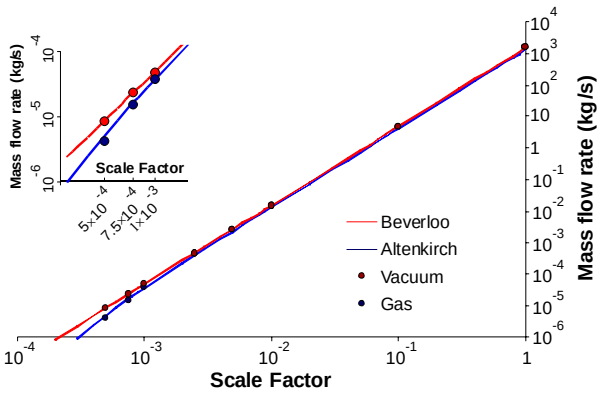

Figure 3: Predicted flow rates vs Beverloo and Altenkirch theoretical relations.

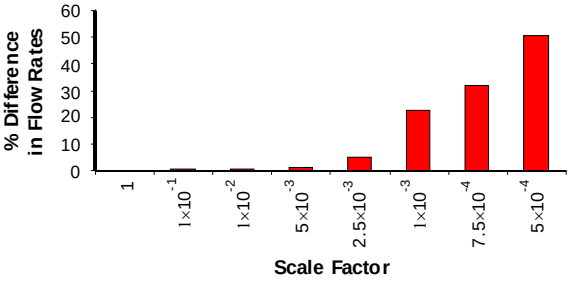

Figure 4: Percentage difference in the flow rates with and without gas flow for different scaling factors.

Fig. 5 shows the axial relative pressure and volume fraction for a closed hopper of scale factor of s = 1.0, at times 1.46, 1.82 and 2.19 s from the start-up of the simulation from the top of the bed, y = +10 m, through the outlet to y = -10 m below the outlet. The hydrostatic pressure, $\rho_f\, g\, y$, has been subtracted from the pressure, giving the dynamic pressure due only to the gas flow. Only a small amount of discharge occurs between these times, and the variation in the dilation over the outlet, as well as the volume fraction at the outlet, remains constant.

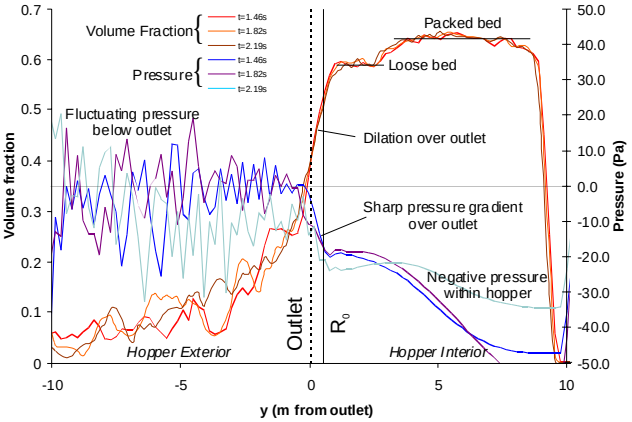

Figure 5: Axial relative pressure and volume fraction for s = 1.0 hopper simulation at 1.46, 1.82 and 2.19 s after start-up.

A packed bed region at the random close packing limit of around 0.64 can clearly be seen on the plot of volume fraction, corresponding to the bulk of the grains in the upper part of the hopper. It can also be seen that substantial dilation occurs over the outlet region with a corresponding sharp pressure gradient. The pressure inside the hopper is negative, which is expected as the particles exiting the hopper draw gas with them, leading to a reduction in the pressure within the hopper. This pressure gradient at the outlet acts against the motion of particles, leading to a reduction in the mass flow rate.

Interestingly, a plateau in the volume fraction occurs just before the free-fall arch, marked as 'loose bed' in Fig. 5. This plateau is common to all scalings and appears to be an intrinsic property of the system. The value of the volume fraction at the plateau is slightly below 0.6 and it therefore seems likely that this point is the granular dilatancy point (Schröter *et al.*, 2007). Most models assume a sharp interface between the bulk volume fraction and the free fall arch. Here, however, the volume fraction falls from the random loose packing limit of around 0.64 to the dilatancy point, but then remains constant until the free fall arch, marked as the vertical R_0 line. This behaviour of the volume fraction upstream from the free fall arch has not been reported before.

GRANULAR DILATION AS A BODY FORCE

It is worth considering the effect of particle dilation on the velocity field of the gas. Neglecting the viscous contribution, Eq. (25) gives:

$$\frac{\partial \mathbf{u}'}{\partial t} + \frac{1}{\varepsilon}\left(\mathbf{u}'\cdot\nabla\right)\mathbf{u}' + \mathbf{u}'\nabla\cdot\frac{\mathbf{u}'}{\varepsilon} = -\frac{\varepsilon\nabla p}{\rho_f} + \frac{\mathbf{f}_{fp}}{\rho_f} + \varepsilon\mathbf{g} \quad (26)$$

If ε is constant with respect to both time and space, Eq. (24) gives $\nabla\cdot\mathbf{u}' = 0$ and Eq. (26) gives an expression very similar to the regular Navier Stokes equations. If, however, ε is *not* constant over space but is constant in time, Eq. (26) gives:

$$\frac{\partial \mathbf{u}'}{\partial t} + \frac{1}{\varepsilon}\left(\mathbf{u}'\cdot\nabla\right)\mathbf{u}' = -\frac{\varepsilon\nabla p}{\rho_f} + \frac{\mathbf{f}_{fp}}{\rho_f} + \varepsilon\mathbf{g} - \mathbf{u}'\left(\mathbf{u}'\cdot\nabla\frac{1}{\varepsilon}\right) \quad (27)$$

The term on the far right hand side, $-\mathbf{u}'(\mathbf{u}'\cdot\nabla\varepsilon^{-1})$, arises from the variation of the voidage fraction in space. It can be considered as an extra body force, $\mathbf{f}_\varepsilon$, in regions with non-zero gradient of voidage fraction. In our system, the dominant granular gradient component and gas velocity is in the y-direction, giving this term as:

$$\frac{\mathbf{f}_\varepsilon}{\rho} = \frac{u_y'^2}{\varepsilon^2}\frac{\partial\varepsilon}{\partial y} \quad (28)$$

The magnitude of this force can be compared with gravity to give a measure of its influence on the system. For the system with s = 1, $|u| \approx 1.0$ m/s, and taking the gradient over the linear portion of the volume fraction from y = 1.2, where $\varepsilon \approx (1 - 0.6)$, to y = -0.5, where $\varepsilon \approx (1 - 0.25)$, gives $\partial\varepsilon/\partial y \approx -0.2$ over the outlet, with an average $\varepsilon \approx 0.575$. This gives $\mathbf{f}_\varepsilon/\rho \approx -0.6$ m/s^2, compared to gravity, $-\varepsilon g \approx -6.0$ m/s^2. The effect of this 'dilationary force' is therefore an increase in the effective gravitational force on the gas of around 10% over the outlet. This dilatancy effect significantly influences the gas and particle dynamics at the outlet. Both this force, as well as the sum of the individual drag forces from the particles on the gas $\mathbf{f}_{fp}$, gives rise to the sharp pressure gradient over the outlet.

CONCLUSION

We have applied a coupled gas and DEM model to the simulation of a flat-bottomed granular hopper and shown that at small length scales gas flow strongly affects the discharge rates. The deviation from the predicted discharge rates in vacuum, given by the Beverloo relation, become important around 500 μm. We have shown that our measured discharge rates agree very closely with the Altenkirch relation.

We have found that a sharp pressure gradient exists over the outlet which is created by the drag on the particles on the gas, as well as a granular dilationary effect. The gas outflow velocity was found to be in the same direction as the particle velocity in the centre of the outflow region, with a thin annular backflow around the outlet. It has previously been suggested that for closed top-hoppers (Altenkirch *et al.*, 1981) the gas flow will be in the opposite direction to the particle flow, leading to $\alpha < 0$, but we have found that the gas dynamics are more complex than this simple assumption. The gas is drawn back into the hopper by the pressure gradient, but takes the path of least resistance. This path is along the minimum volume fraction, which is the annular region between the particle bulk and the outlet plate.

We have also observed a granular transition above the free fall arch which has not previously been taken into account in the granular flow theories applied to hopper discharge. Our model and findings will be of interest to industrial applications involving fine powders, such as bin discharge, feeding, and die filling, as well as a theoretical perspective for new models of the interaction of dense granular flows with gas effects.

REFERENCES

ABOU-CHAKRA,, H. BAXTER, J., AND TUZUN, U., (2004), "Three-dimensional shape descriptors for computer simulation of non-spherical particulate assemblies", *Adv. Powder Tech*., **1**, p63

ALTENKIRCH, R. A. and EICHHORN, R., (1981), "Effect of fluid drag on low Reynolds number discharge of solids from a circular orifice", *AIChE Journal*, **27**, p593

ANAND, A., CURTIS, J. S., WASSGREN, C. R., HANCOCK, B.C., KETTERHAGEN, W.R., (2008), "Predicting discharge dynamics from a rectangular hopper using the discrete element method (DEM)", *Chem. Eng. Sci.*, **63**, p5821

ANDERSON, T.B. and JACKSON, R., (1967), "A fluid mechanical description of fluidised beds", *Industrial and Engineering Chemistry Fundamentals*, **6**, p527

BARLETTA, D., DONSI, G., FERRARI, G., POLETTO, M., (2003), "On the role and the origin of the gas pressure gradient in the discharge of fine solids from hoppers", *Chem. Eng. Sci.*, **58**, p5269

BEVERLOO, W. A., LENIGER, H. A., VANDEVELDE, J., (1961), "The flow of granular solids through orifices". *Chem. Eng. Sci.*, **15**, p260

BROWN, R. L., RICHARDS, J. C., (1960), *Trans. Inst. Chem. Eng.*, **38**, p243

BROWN, R. L., (1961) "Minimum energy theorem for flow of dry granules through apertures", *Nature*, **191**, p458

BROWN, R. L., RICHARDS, J. C., (1965), "Kinematics of the flow of dry powders and bulk solids", *Rheologica Acta*, **4**, p153

BULSARA, P. U., ZENZ, F. A., ECKERT, R. S., (1964), *Ind. Eng. Chem. Proc. Des. Dev.*, **3**, p348.

CARLETON A.J., (1972), "The effect of fluid-drag forces on the discharge of free-flowing solids from hoppers", *Powder Tech.*, **6**, p91

CLEARY, P.W., SAWLEY, M.L., (2002), "DEM modelling of industrial granular flows: 3D case studies and the effect of particle shape on hopper discharge", *App. Math. Mod.*, **26**, p89

CLEARY, P.W., (2009), "Industrial particle flow modeling using discrete element method", Engineering Computations, 26, p698

CLEARY, P.W., (2004), "Large scale industrial DEM modelling" , *Engineering Computations*, **21**, p169

CREWDSON, B. J., ORMOND, A.L., NEDDERMAN, R.M., (1977), "Air-impeded discharge of fine particles from a hopper", *Powder Tech.*, **16**, p197

CUNDALL, P. A. and STRACK, O. D. L., (1979), "A discrete numerical model for granular assemblies", *Geotechnique*, **29**, p47

Di FELICE, R., (1994) "The voidage function for fluid-particle interaction systems", *Int. J. Multiphase Flow*, **20**, p153

DONSI, G., FERRARI, G., POLETTO, M., (1997), "Distribution of gas pressure inside a hopper discharging fine powders", *Chem. Eng. Sci.*, **52**, p4291

GUO, Y., KAFUI, K. D., WU, C. Y., THORNTON, C., SEVILLE, J. P. K., (2009), "A coupled DEM/CFD analysis of the effect of air on powder flow during die filling", *AIChE*, **55**, p49

HARMENS, A., (1963), "Flow of granular material through horizontal apertures", *Chem. Eng. Sci.*, **18**, p297

HÖLZER, A. and SOMMERFELD, M., (2008), "New simple correlation formula for the drag coefficient of non-spherical particles", *Powder Technology*, **184**, p361

JANSSEN, H. A., (1895), *Z. Ver. dt. Ing.*, **39**, p1045

KAFUI, D. K., THORNTON and C. ADAMS, M. J., (2002), "Discrete particle-continuum fluid modelling of gas-solid fluidised beds", *Chem. Eng. Sci.*, **57**, p2395

KAZA, K. R., JACKSON, R., (1984), "Boundary conditions for a granular material flowing out of a hopper or bin", *Chem. Eng. Sci.*, **39**, p915

KETCHUM, M. S., (1929), "The Design of Walls, Bins and Grain Elevators", *McGraw-Hill*, New York

LANGSTON, P. A., TUZUN, U., HEYES, D. M., (2005), "Distinct element simulation of interstitial air effects in axially symmetric granular flows in hoppers", *Chem. Eng. Sci.*, **51**, p873

LIA, J., LANGSTON, P. A., WEBB, C., DYAKOWSKI, T., (2004), "Flow of sphero-disk particles in rectangular hoppers - a DEM and experimental comparison in 3D", *Chem. Eng. Sci.*, **59**, p5917

LEUNG, L. S., JONES, P. J., KNOWLTON, T. M., (1978), *Trans. Soc. Rheology*, **18**, p247

MCDOUGALL, I. R., EVANS, A. C., (1966), *Trans. Inst. Chem. Eng.*, **44**, 15.

NEDDERMAN, R. M., TUZUN, U., SAVAGE, S. B., HOULSBY, G.T., (1982), "The flow of granular materials-I: Discharge rates from hoppers", *Chem. Eng. Sci.*, **37**, p1597

NEDDERMAN, R. M., TUZUN, U., THORPE, R. B., (1983), "The effect of interstitial air pressure gradients on the discharge from bins", *Powder Tech.*, **35**, p69

NEDDERMAN, R. M., (1992), *Statics and Kinematics of Granular Materials*, Cambridge University Press

RESNICK, W., (1972), *Trans. Inst. Chem. Eng.*, **50**, p289

SCHRÖTER, M., NAGLE, S., RADIN, C. and SWINNEY, H. L., (2007), "Phase transition in a static granular system", *EPL*, **78**, 44004

SEVILLE, J.P.K., TUZUN, U., CLIFT, R., 1997. *Processing of Particulate Solids*, Blackie Academic & Professional

SNIDER, D. M., (2007), "Three fundamental granular flow experiments and CPFD predictions", *Powder Tech.*, **176**, p36

TSUJI, Y., KAWAGUCHI, T., TANAKA, T., (1993), "Discrete particle simulation of two-dimensional fluidized bed", *Powder Tech.*, **77**, p79

WIEGHARDT, K., (1975), "Experiments in Granular Flow", *Annual Review of Fluid Mechanics*, **7**, p89

WU, J., BINBO, J., Chen, J., YANG, Y., (2009), "Multi-scale study of particle flow in silos", *Adv. Powder Tech.*, **20**, p62

ZHU, H. P., YU, A. B., (2004), "Steady-state granular flow in a three-dimensional cylindrical hopper with flat bottom, microscopic analysis", *J. Phy. D.*, **37**, p1497